
Article:
Lade, Rachel E., Blitz, Mark A., Rowlinson, Matthew et al. (3 more authors) (2024) Kinetics of the reactions of the Criegee intermediate CH2OO with water vapour:experimental measurements as a function of temperature and global atmospheric modelling. Environmental Science: Atmospheres. pp. 1294-1308. ISSN 2634-3606

https://doi.org/10.1039/d4ea00097h

Environmental Science: Atmospheres

ROYAL SOCIETY OF CHEMISTRY

PAPER

View Article Online
View Journal | View Issue

Cite this: *Environ. Sci.: Atmos.*, 2024, **4**, 1294

Kinetics of the reactions of the Criegee intermediate CH_2OO with water vapour: experimental measurements as a function of temperature and global atmospheric modelling†

Rachel E. Lade,[a] Mark A. Blitz,[ab] Matthew Rowlinson,[c] Mathew J. Evans,[cd] Paul W. Seakins[a] and Daniel Stone *[a]

The kinetics of reactions between the simplest Criegee intermediate, CH_2OO, and water vapour have been investigated at temperatures between 262 and 353 K at a total pressure of 760 Torr using laser flash photolysis of CH_2I_2–O_2–N_2–H_2O mixtures coupled with broadband time-resolved UV absorption spectroscopy. Results indicate that the reaction with water monomers represents a minor contribution to the total loss of CH_2OO under the conditions employed in this work, with an estimated rate coefficient for $CH_2OO + H_2O$ (R1) of $(9.8 \pm 5.9) \times 10^{-17}$ cm^3 molecule^{-1} s^{-1} at 298 K and a temperature dependence described by $k_1 = (3.2 \pm 1.1) \times 10^{-13} \exp(-(2410 \pm 270)/T)$ cm^3 molecule^{-1} s^{-1}. The reaction of CH_2OO with water dimers, $CH_2OO + (H_2O)_2$ (R2), dominates under the conditions employed in this work. The rate coefficient for R2 has been measured to be $k_2 = (9.5 \pm 2.5) \times 10^{-12}$ cm^3 molecule^{-1} s^{-1} at 298 K, with a negative temperature dependence described by $k_2 = (2.85 \pm 0.40) \times 10^{-15} \exp((2420 \pm 340)/T)$ cm^3 molecule^{-1} s^{-1}, where $\text{rate}_{R2} = k_2[CH_2OO][(H_2O)_2]$. For use in atmospheric models, we recommend description of the kinetics for R2 in terms of the product of the rate coefficient k_2 and the equilibrium constant K_{eq}^D ($k_{2,eff} = k_2K_{eq}^D$) for water dimer formation to allow the rate of reaction to be expressed in terms of water monomer concentration as $\text{rate}_{R2} = k_{2,eff}[CH_2OO][H_2O]^2$ to avoid explicit calculation of dimer concentrations and impacts of differences in values of K_{eq}^D reported in the literature. Results from this work give $k_{2,eff} = (1.96 \pm 0.51) \times 10^{-32}$ cm^6 molecule^{-2} s^{-1} at 298 K with a temperature dependence described by $k_{2,eff} = (2.78 \pm 0.28) \times 10^{-38} \exp((4010 \pm 400)/T)$ cm^6 molecule^{-2} s^{-1}. No significant impacts of a reaction between CH_2OO and three water molecules were observed in this work, potentially as a result of the relative humidities used in this work (up to 57% at 298 K). Atmospheric implications of the results have been investigated using the global chemistry transport model GEOS-Chem. Model simulations indicate that the reaction with water dimers dominates the loss of CH_2OO in the atmosphere and limits the impacts of other reactions of CH_2OO, with the reaction with water dimers representing >98% of the total loss of CH_2OO in the troposphere.

Received 5th July 2024
Accepted 29th September 2024

DOI: 10.1039/d4ea00097h

rsc.li/esatmospheres

Environmental significance

Criegee intermediates are key species in atmospheric chemistry, produced following the ozonolysis of unsaturated volatile organic compounds. The chemistry of Criegee intermediates influences atmospheric composition, and as a consequence, air quality and climate. The reactions of the simplest Criegee intermediate CH_2OO with water monomers and dimers are expected to dominate its atmospheric chemistry, but there have been few experimental studies over a range of conditions relevant to the atmosphere. In our work we have performed a detailed experimental study of the kinetics of CH_2OO reactions with water monomers and dimers over a wide range of temperatures relevant to the atmosphere, with atmospheric impacts of the reactions determined using the global chemistry transport model GEOS-Chem.

[a]*School of Chemistry, University of Leeds, Leeds, LS2 9JT, UK. E-mail: d.stone@leeds.ac.uk*
[b]*National Centre for Atmospheric Science, University of Leeds, Leeds, LS2 9JT, UK*
[c]*Wolfson Atmospheric Chemistry Laboratories, Department of Chemistry, University of York, York YO10 5DQ, UK*
[d]*National Centre for Atmospheric Science, University of York, York YO10 5DQ, UK*

† Electronic supplementary information (ESI) available: Hygrometer calibration and measurements of water vapour; description of the instrument response function; mixed-order analysis; concentration–time profiles for CH_2I_2 and IO; description of the analysis in terms of $k_{2,eff}$ and use of literature values for K_{eq}^D; investigation of the potential reaction between CH_2OO and three water molecules; experimental uncertainties; comparison of global and local fit results for $k_{2,eff}$; comparison of observations with previous work; values for k_1 and $k_{2,eff}$ used in GEOS-Chem simulations; summary of experimental data. See DOI: https://doi.org/10.1039/d4ea00097h

Introduction

Criegee intermediates (CIs) are reactive zwitterionic species with the general formula R_1R_2COO produced in the atmosphere following the ozonolysis of unsaturated volatile organic compounds (VOCs). Ozonolysis reactions are typically exothermic by ~250–300 kJ mol^{-1}, producing CIs with high internal energies.[1] The nascent CI may undergo unimolecular decomposition to form important trace species such as OH, HO_2 and CO,[2] or stabilisation through collisional energy transfer with surrounding gas molecules to form stabilised Criegee intermediates (SCIs). SCIs have longer atmospheric lifetimes than the nascent excited CIs, allowing them to participate in a wide range of chemical reactions. Bimolecular reactions of SCIs with water vapour[3,4] and SO_2 [5,6] are of particular interest as they have the potential to impact atmospheric budgets of secondary organic aerosols (SOA), gas phase sulfuric acid, and sulfate aerosol, thereby influencing air quality and climate. Reaction with water vapour is expected to dominate the atmospheric chemistry of the simplest SCI, CH_2OO, but there is uncertainty over the role of reactions involving water monomers (H_2O, R1), water dimers ($(H_2O)_2$, R2), or potentially three water molecules (likely *via* $CH_2OO{\cdot}H_2O + (H_2O)_2$ or $CH_2OO{\cdot}(H_2O)_2 + H_2O$, represented as $CH_2OO + 3H_2O$ in R3) with a wide range of values reported for the kinetics of R1 and R2 [7–10] and significant uncertainties regarding the products and product yields.[11–15]

$$CH_2OO + H_2O \rightarrow \text{Products} \quad \text{(R1)}$$

$$CH_2OO + (H_2O)_2 \rightarrow \text{Products} \quad \text{(R2)}$$

$$CH_2OO + 3H_2O \rightarrow \text{Products} \quad \text{(R3)}$$

The development of photolytic precursors for the production of Criegee intermediates,[16,17] including CH_2OO,[18,19] has led to the development of direct detection techniques for Criegee intermediates and improvements in our understanding of the reaction kinetics of a number of Criegee intermediate reactions relevant to the atmosphere.[5,20,21] Welz *et al.*[18] produced CH_2OO following the 248 nm laser flash photolysis of diiodomethane, CH_2I_2, and investigated its potential reaction with water vapour, using tuneable VUV synchrotron photoionisation mass spectrometry (PIMS), at a total pressure of 4 Torr. Welz *et al.* observed no significant change in the decay of CH_2OO on addition of water vapour at concentrations up to 3.1×10^{16} molecule cm^{-3}, leading to the conclusion of an upper limit for k_1 of 4×10^{-15} cm^3 $molecule^{-1}$ s^{-1} at 298 K. A subsequent study by Ouyang *et al.*[22] examined the impact of water vapour on the production of NO_3 following the 248 nm photolysis of CH_2I_2–O_2–N_2–NO_2 mixtures, based on the assumption that NO_3 was produced *via* $CH_2OO + NO_2$, which suggested a reaction of CH_2OO with water vapour. However, a number of studies have since indicated that NO_3 is produced *via* secondary chemistry in the system,[4,23] leading to uncertainty in the result.

Photolytic production of CH_2OO was also used by Stone *et al.*[5] in a series of experiments monitoring the production of formaldehyde, HCHO, from CH_2OO reactions *via* laser-induced fluorescence (LIF) spectroscopy. No significant change in the rate of HCHO production was observed on addition of water vapour at concentrations up to 1.7×10^{17} molecule cm^{-3} at a total pressure of 200 Torr, with a small change in HCHO yield attributed to fluorescence quenching by water and results indicating an upper limit of 9×10^{-17} cm^3 $molecule^{-1}$ s^{-1} for k_1 at 295 K.

The effects of water vapour on CH_2OO chemistry have also been investigated in studies of ozonolysis reactions through the competition with the reaction of CH_2OO with SO_2.[7,8] Berndt *et al.*[3] monitored the production of sulfuric acid, which is produced rapidly following the production of SO_3 *via* $CH_2OO + SO_2$,[24–26] during ethene ozonolysis experiments conducted in a flow tube at 293 K over a range of water vapour concentrations. A quadratic relationship was observed between the rate coefficient describing the loss of CH_2OO and the water monomer concentration, with a linear relationship demonstrated with the concentration of water dimers, $(H_2O)_2$, indicating that the dominant reaction of CH_2OO was with water dimers (R2) rather than water monomers (R1). Berndt *et al.* reported a value of $k_2 = (1.07 \pm 0.04) \times 10^{-11}$ cm^3 $molecule^{-1}$ s^{-1}. Later work by Berndt *et al.*[27] investigated the kinetics of CH_2OO reactions in the presence of water vapour using a free-jet flow system at 297 K by detecting H_2SO_4 formed following the reaction of CH_2OO with SO_2, and reported $k_1 = (3.2 \pm 1.2) \times 10^{-16}$ cm^3 $molecule^{-1}$ s^{-1}. Newland *et al.*[10] also investigated the impact of water vapour on $CH_2OO + SO_2$ by monitoring the consumption of SO_2 in ethene ozonolysis experiments at the EUPHORE atmospheric simulation chamber, with results also indicating a more rapid reaction of CH_2OO with water dimers than water monomers and giving $k_1 = (1.2 \pm 0.4) \times 10^{-15}$ cm^3 $molecule^{-1}$ s^{-1} and $k_2 = (5.2 \pm 6.7) \times 10^{-13}$ cm^3 $molecule^{-1}$ s^{-1} at 298 K using the current IUPAC recommendation of 3.7×10^{-11} cm^3 $molecule^{-1}$ s^{-1} for the rate coefficient for the reaction of CH_2OO with SO_2.

Direct measurements of CH_2OO have also been made in the presence of excess water vapour using laser flash photolysis of CH_2I_2–O_2–N_2–H_2O mixtures coupled with time-resolved broadband UV absorption spectroscopy.[15,28] Results from several studies have now demonstrated a quadratic dependence of the pseudo-first-order rate coefficient describing the loss of CH_2OO on the water vapour concentration[4,15,28,29] thus also indicating that the reaction of CH_2OO with water dimers dominates over reaction with water monomers. Lewis *et al.*[4] reported a rate coefficient for reaction of CH_2OO with water dimers of $(4.0 \pm 1.2) \times 10^{-12}$ cm^3 $molecule^{-1}$ s^{-1} at 294 K, with no significant dependence on pressure in the range 50 to 400 Torr. Chao *et al.*[28] reported a value for k_2 of $(6.5 \pm 0.8) \times 10^{-12}$ cm^3 $molecule^{-1}$ s^{-1} at 298 K that also showed no significant dependence on pressure between 100 and 500 Torr.

The temperature dependence of k_2 was subsequently investigated by Smith *et al.*[29] using UV absorption spectroscopy between 283 and 324 K, with results giving $k_2 = (7.4 \pm 0.6) \times 10^{-12}$ cm^3 $molecule^{-1}$ s^{-1} at 298 K, in agreement with the work of Chao *et al.*,[28] and a negative temperature dependence.[30] Further experiments have been performed using UV absorption spectroscopy by Wu *et al.*[31] at temperatures between 290 and 346 K, which showed high precision in measurements of water

vapour concentrations and CH_2OO signal and led to the conclusion that observed kinetics of CH_2OO removal in the presence of water vapour result from a combination of reactions involving one, two, or three water molecules. Experiments by Wu *et al.* were carried out at higher relative humidities than those employed in other studies, reaching close to 100% at each temperature investigated, and Wu *et al.* reported that the measurements at the highest relative humidities correspond to reaction with three water molecules, most likely involving $CH_2OO{\cdot}H_2O + (H_2O)_2$ or $CH_2OO{\cdot}(H_2O)_2 + H_2O$ rather than a direct reaction of CH_2OO with water trimers ($(H_2O)_3$), while experiments at low relative humidity provided information relating to the reaction with the water monomer. Wu *et al.* reported a positive temperature dependence for the reaction of CH_2OO with the water monomer, and a negative temperature dependence for the reaction of CH_2OO with water dimers that is in broad agreement with the behaviour observed by Smith *et al.*[29] The reaction involving three water molecules also displayed a negative temperature dependence, with results indicating that this reaction could play an important role at high relative humidities at temperatures of 298 K and below.

There is a growing consensus that chemistry of CH_2OO in the presence of water vapour is rapid, with a significant role for a reaction with water dimers, which, despite low water dimer concentrations (3.0×10^{14} molecule cm^{-3} for a relative humidity of 50% at 298 K) compared to water monomers in the atmosphere, is likely to dominate atmospheric losses of CH_2OO. Although the study by Welz *et al.*[18] did not observe any evidence for the reaction between CH_2OO and water dimers, the water dimer concentrations at the low pressure (4 Torr) used by Welz *et al.* would have limited the impact of the reaction. The HCHO LIF experiments performed by Stone *et al.*[5] did enable the use of higher water vapour concentrations, and thus significant water dimer concentrations. However, the impact of water vapour on production of HCHO may have been limited if HCHO is not a direct product of CH_2OO reactions with water, and the reduction in HCHO signal which was attributed to quenching may have resulted from the production of other products. Product studies in ozonolysis reactions have reported the formation of HCHO, among other potential products,[13,32] but more recent time-resolved product measurements, using laser flash photolysis of CH_2I_2–O_2 in the presence of water vapour, have observed the production of hydroxymethyl hydroperoxide ($HOCH_2OOH$, HMHP) by rotational spectroscopy[33] and PIMS,[15] with the PIMS study indicating HMHP as the dominant product of R1 and R2.[15] Theory[34–44] has also indicated that HMHP is a major product of R1 and R2, and supports the experimental results which suggest the dominant reaction is with water dimers. Subsequent chemistry of HMHP can lead to the production of formic acid (HCOOH), H_2O_2, and HCHO, which has been investigated by Nguyen *et al.*[13] using measurements made in an atmospheric simulation chamber at 295 K and 1 atm at relative humidities between 4 and 76%. Measurements of HCHO, OH and HO_2 were made in the chamber using LIF spectroscopy,[45] while hydroperoxides (such as HMHP) and acids (such as HCOOH) were measured by chemical ionisation mass spectrometry (CIMS). At relative humidities below ~40%, HMHP was observed to be the dominant product, followed by HCOOH and H_2O_2. However, at relative humidities above ~40%, Nguyen *et al.* observed a significant decrease in the yield of HMHP, accompanied by an increase in the yield of HCOOH. Modelling of the observed yields for HMHP and HCOOH led to the conclusion that R1 leads to production of 73% HMHP, 21% HCOOH + H_2O, and 6% HCHO + H_2O_2, while R2 leads to production of 54% HCOOH + H_2O, 40% HMHP, and 6% HCHO + H_2O_2. The product distribution reported by Nguyen *et al.* forms the basis of the current mechanism adopted in the global atmospheric chemistry transport model (CTM) GEOS-Chem.

There is general agreement regarding the atmospheric significance of CH_2OO reactions involving water, but there are discrepancies in product distributions and measured kinetics at room temperature, and the temperature dependence of the kinetics has only been investigated over a relatively narrow temperature range. In this work we report the results of experiments performed using laser flash photolysis of CH_2I_2–O_2–N_2–H_2O mixtures coupled with time-resolved broadband UV absorption spectroscopy at temperatures in the range 262 to 353 K at 760 Torr. We also report atmospheric implications of the experimental results based on GEOS-Chem model simulations of CH_2OO chemistry.

Experimental

The kinetics of CH_2OO loss in the presence of water vapour have been studied as a function of temperature between 262 and 353 K at 760 Torr, using laser flash photolysis of CH_2I_2–O_2–N_2–H_2O gas mixtures coupled with time-resolved broadband UV absorption spectroscopy. The experimental apparatus has been described in detail previously[21,46] and so only a brief overview is given here.

Gases (N_2 (BOC, 99.998%) and O_2 (BOC, 99.5%)) were mixed in a gas manifold at known concentrations using calibrated mass flow controllers (MFCs). Water vapour was added to the system by passing a known flow of N_2 gas through a bubbler containing deionised water held in a water bath at 70 °C. The concentration of water vapour was measured at the exit of the reaction cell by a relative humidity (RH) probe (Michell Instruments PCMini52) that was calibrated against a dew point hygrometer (Buck Research Instruments, CR-4 chilled mirror hygrometer) (see ESI† for further details). The precursor CH_2I_2 (Alfa Aesar, 99%) was introduced into the gas mixture by flowing a fraction of the N_2–O_2–H_2O flow over liquid CH_2I_2 contained in a bubbler before combining with the remaining N_2–O_2–H_2O flow and passing the gas mixture into the reaction cell. The concentration of CH_2I_2 in the gas mixture could be controlled by a needle valve placed before the bubbler and was determined experimentally by measuring the UV intensity transmitted through the cell in experiments with and without CH_2I_2 present in the gas mixture flowing through the cell. Experiments were performed under pseudo-first-order conditions. Initial concentrations were: $[H_2O] = (0–5.5) \times 10^{17}$ molecule cm^{-3}, $[CH_2I_2] = (3.8–6.4) \times 10^{13}$ molecule cm^{-3}, and $[O_2] = (1.2–2.7) \times 10^{18}$ molecule cm^{-3}.

The reaction cell was a 100 cm long jacketed glass tube with an inner diameter of 3 cm and fused silica windows at both ends. Experiments were carried out at temperatures between 262 and 353 K, with the temperature of the system controlled by circulating a thermofluid (HUBE6479 DW-THERM) from a thermoregulator (Huber Unistat 360) through the outer jacket of the cell. The temperature of the system was calibrated by flowing N_2 through the reaction cell, under conditions identical to those used in kinetic experiments, and measuring the temperature using a K-type thermocouple at 5 cm increments along the length of the reaction cell.[20] The total flow rate in the cell was 3700 sccm (standard cm^3min^{-1}), giving a residence time in the cell of 13.1 s, with relatively slow flows required in order to maximise saturation of the gas flow as it passed through the water bubbler. Experiments were performed at a total pressure of 760 Torr, which was controlled by throttling the exit of the cell to the pump and measured by a capacitance manometer (MKS instruments).

Chemistry was initiated using an excimer laser (KrF, Lambda-Physik CompEx 210) operating at a wavelength of 248 nm with a typical laser fluence of 15–25 mJ cm^{-2}, giving initial CH_2OO concentrations in the range $(2.0–8.3) \times 10^{11}$ molecule cm^{-3}. The pulse repetition rate was set at 0.075 Hz to ensure there was enough time for a fresh gas mixture to be introduced to the reaction cell before the laser fired again.

UV light for the absorption measurements was provided by a laser-driven light source (LDLS, Energetiq EQ-99X) that provided ~10 mW cm^{-2} of light at wavelengths between 200 and 800 nm. The light was collimated using an off-axis parabolic mirror (ThorLabs MPD129-F01 UV enhanced aluminium) and multi-passed nine times through the reaction cell by ten Al mirrors (Knight optical MCQ1200-C concave mirror UV enhanced, reflectivity >85% in the UV), each of 12 mm diameter, which were positioned outside the windows of the cell on a custom mirror mount.[46] Each mirror in the multipass arrangement could be adjusted to align the probe beam such that there is maximum overlap with the 248 nm excimer beam, giving a total effective path length of $l = (595 \pm 53)$ cm (details regarding the determination of the effective path length are described in our previous work[20]).

In order to reduce the detection of scattered light from the photolysis laser, the probe beam exiting the cell was passed through a sharp cut-on filter (RazorEdge ultrasteep long-pass edge filter 248 nm), which effectively blocks light at wavelengths below 250 nm, and focussed onto a fibre optic. The fibre optic directed light through a 25 μm slit onto a spectrograph with a diffraction grating of 600 grooves mm^{-1} (Princeton Instruments, FER-GRT-060-500) which imaged the light onto a charge-coupled device (CCD) (Princeton Instruments, FER-SCI-1024BRX) detector with a spectral resolution (full width half maximum (FWHM)) of 1.1 nm. The CCD was cooled to −45 °C by a Peltier device to reduce the effects of dark current, and, prior to the start of experiments, a background spectrum was also measured to account for any remaining dark current on the device.

Light was imaged onto ten of rows on the CCD and transferred at specified time intervals either directly to the PC for analysis for measurements of stable gas mixtures, or onto a storage region on the CCD for time resolved measurements before transfer to the PC for analysis. The typical time resolution of kinetic experiments ranged between 70 μs and 165 μs (typically much shorter than the ms timescale of the kinetic decays), with the measurement and transfer to the storage region on the CCD leading to a Gaussian instrument response function (IRF) that has been described in previous work[21] and was accounted for during data analysis. The intensity data for time-resolved experiments were typically averaged over 125 photolysis shots, with the time delay between the operation of the camera and the firing of the excimer laser controlled by a delay generator (SRS model DG 535).

The absorbance, $A_{\lambda,t}$, was determined for each wavelength λ and time point t from the measured intensities using the Beer–Lambert Law (eqn (1)):

$$A_{\lambda,t} = \ln\left(\frac{I_{\lambda,0}}{I_{\lambda,t}}\right) = \sum_i \sigma_{i,\lambda}[i]_t l \quad (1)$$

where $I_{\lambda,0}$ is the average intensity at wavelength λ before photolysis ($t = 0$), $I_{\lambda,t}$ is the intensity at wavelength λ at time t, $\sigma_{i,\lambda}$ is the absorption cross-section of species i at wavelength λ, $[i]_t$ is the concentration of species i at time t, and l is the effective path length of light ((595 ± 53) cm in this work).

Fig. 1 shows a typical absorbance spectrum observed following photolysis, which contains contributions from the Criegee intermediate, CH_2OO, the CH_2I_2 precursor (which exhibits a negative absorbance owing to depletion on photolysis), and iodine monoxide (IO) radicals which are produced in the system as a result of secondary chemistry.[21,49] Reference spectra for CH_2OO,[21] CH_2I_2 [47] and IO[48] were interpolated onto the experimental wavelength grid and least squares fit to the total observed absorbance using eqn (1) to determine the concentration of each species at each time point. Fig. 1 also

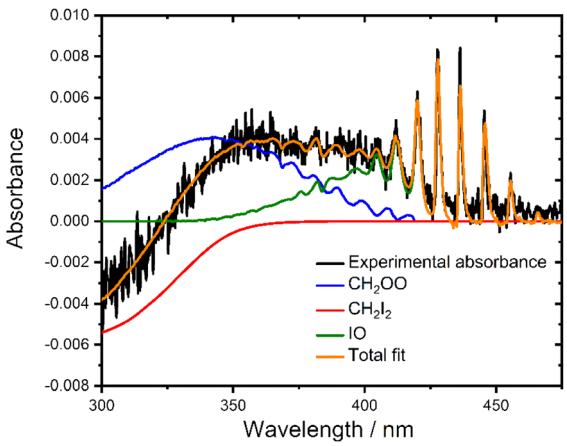

Fig. 1 Observed absorbance (black), total fit (orange) and individual contributions of CH_2OO[21] (blue), CH_2I_2 [47] (red) and IO[48] (green) obtained by performing a least squares fit of reference cross-sections to the observed absorbance at $t = 1$ ms after photolysis at $p = 760$ Torr and $T = 298$ K with $[CH_2I_2]_0 = 4.1 \times 10^{13}$ molecule cm^{-3}. $[CH_2OO]_t = 6.4 \times 10^{11}$ molecule cm^{-3}, $\Delta[CH_2I_2]_t = -3.8 \times 10^{12}$ molecule cm^{-3} and $[IO]_t = 7.3 \times 10^{11}$ molecule cm^{-3}.

shows a typical fit to the observed absorbance following photolysis.

Results

Fig. 2 shows typical concentration–time profiles for CH_2OO for a range of water vapour concentrations, demonstrating a more rapid loss of CH_2OO as the water vapour concentration is increased. Experiments were performed under pseudo-first-order conditions, with water vapour concentrations in excess over CH_2OO, and the temporal behaviour of CH_2OO thus described by eqn (2).

$$[CH_2OO]_t = [CH_2OO]_0 \exp(-k't) \quad (2)$$

where k' represents the sum of the first-order, or pseudo-first-order, rate coefficients describing the loss of CH_2OO. Eqn (2), convoluted with the instrument response function (see ESI† for further details), was fit to concentration–time profiles to determine k'. Losses in the absence of water, which are dominated by the CH_2OO self-reaction,[21] and reactions with IO[21] or iodine atoms,[21] are approximated as being first-order in this work.[20,28,29] Results are shown in Fig. 2, with the fit quality indicating that the data are well-described by pseudo-first-order kinetics. In addition, data were also analysed with a mixed first- and second-order model (see ESI† for further details). No significant differences between the first-order component obtained from the mixed-order model and those obtained from the pseudo-first-order model (eqn (2)) in the presence of water vapour were found, suggesting that the approximation of losses in the absence of water vapour as being first-order is valid for the conditions employed in this work.

Fig. 3 shows that there is a non-linear dependence of the observed pseudo-first-order rate coefficients (k'), obtained by fitting with eqn (2), on the water vapour concentration. Similar behaviour has been observed in previous work, with the non-linear dependence attributed to reaction of CH_2OO with water dimers (R2)[3,4,10,15,28,31,50] or a reaction involving three water molecules (R3)[31] dominating over the reaction of CH_2OO with water monomers (R1). For a system involving reactions R1, R2, and R3, the observed pseudo-first-order rate coefficients k' are given by eqn (3):

$$k' = k_0 + k_1' + k_2' + k_3' \quad (3)$$

where the rate coefficient k_0 refers to the loss of CH_2OO in the absence of water (which is approximated here as being pseudo-first-order, see ESI†) and k_1', k_2', and k_3' are the pseudo-first-order rate coefficients for R1, R2, and R3, respectively. We define k_2 as the bimolecular rate coefficient for R2, which involves explicit calculation of the dimer concentration in $\text{rate}_{R2} = k_2[CH_2OO][(H_2O)_2]$, and $k_{2,\text{eff}}$ as an effective rate coefficient given by the product of k_2 and the equilibrium constant for dimer formation (K_{eq}^D), such that $\text{rate}_{R2} = k_2K_{eq}^D[CH_2OO][H_2O]^2 = k_{2,\text{eff}}[CH_2OO][H_2O]^2$. This removes the need for explicit calculation of the water dimer concentration and allows for simpler parameterisation of the kinetics for use in atmospheric models which relies only on the monomer concentration. For R3, we define $k_{3,\text{eff}}$ such that $\text{rate}_{R3} = k_{3,\text{eff}}[CH_2OO][H_2O]^3$ which removes need for knowledge of the exact reaction mechanism, *i.e.* whether the reaction proceeds *via* $CH_2OO{\cdot}H_2O + (H_2O)_2$ or $CH_2OO{\cdot}(H_2O)_2 + H_2O$. The quadratic and cubic relationships with water monomer concentrations for R2 and R3, respectively, lead to the potential for the observed non-linear dependence of k' on the water monomer concentration.

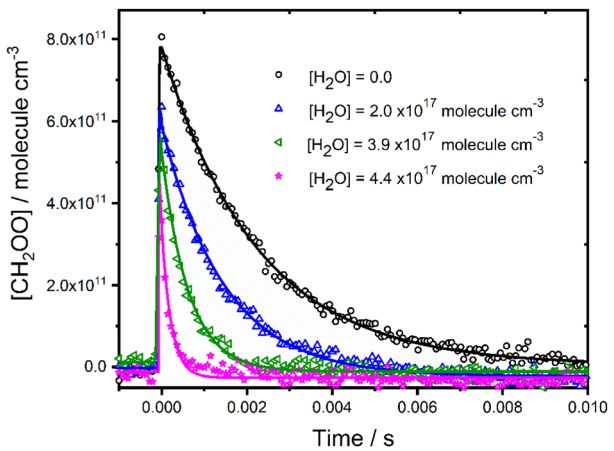

Fig. 2 Concentration–time profiles for CH_2OO in the presence and absence of water vapour at $p = 760$ Torr and $T = 298$ K. Solid lines represent unweighted fits to eqn (2) convoluted with the instrument response function. For $[H_2O] = 0$, the fit gave $[CH_2OO]_0 = 8.3 \times 10^{11}$ molecule cm^{-3} and $k' = (313 \pm 7)$ s^{-1}; for $[H_2O] = 2.0 \times 10^{17}$ molecule cm^{-3}, the fit gave $[CH_2OO]_0 = 6.6 \times 10^{11}$ molecule cm^{-3} and $k' = (1247 \pm 37)$ s^{-1}; for $[H_2O] = 3.9 \times 10^{17}$ molecule cm^{-3}, the fit gave $[CH_2OO]_0 = 5.8 \times 10^{11}$ molecule cm^{-3} and $k' = (2669 \pm 120)$ s^{-1}; for $[H_2O] = 4.4 \times 10^{17}$ molecule cm^{-3}, the fit gave $[CH_2OO]_0 = 5.7 \times 10^{11}$ molecule cm^{-3} and $k' = (3722 \pm 245)$ s^{-1}.

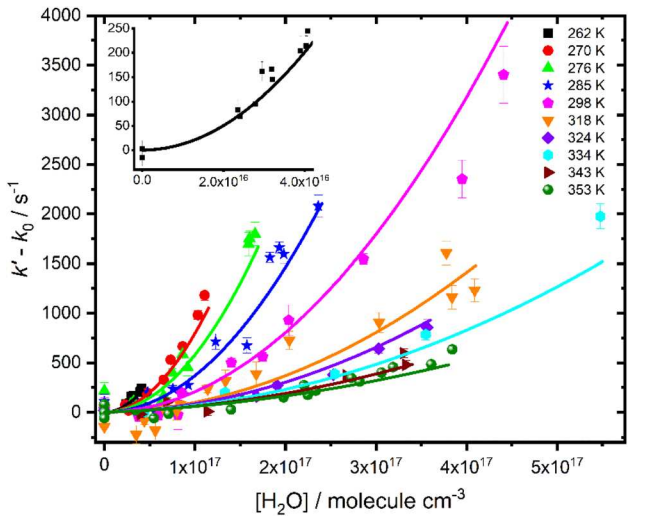

Fig. 3 Pseudo-first-order rate coefficients as a function of water monomer concentration for experiments carried out at 760 Torr and temperatures between 262 and 353 K. The solid lines represent an unweighted global fit to eqn (3). The error bars represent the error in the fits to eqn (2). The inset shows data from experiments carried out at 262 K for clarity. Data for each temperature are shown separately in the ESI.†

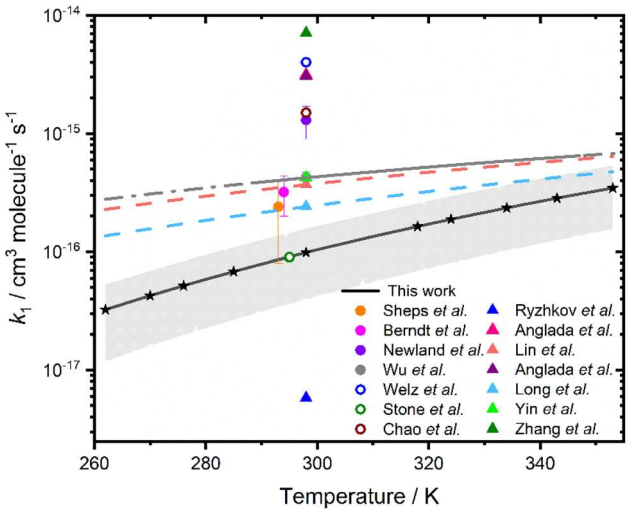

Fig. 4 Rate coefficients k_1 as a function of temperature. The global fit to results obtained in this work is shown by the solid black line, with uncertainties determined from a combination of the statistical error and the systematic errors resulting from uncertainties in gas flow rates and in the concentration of [H_2O] shown by the shaded region. Stars represent the temperatures at which measurements were made. Results from previous studies are also included, where filled circles represent experimentally measured rate coefficients,[10,15,27,31] hollow circles represent experimentally determined upper limits,[5,18,28] and triangles represent rate coefficients calculated from theory.[34–38,41,44] The solid grey line shows the data reported by Wu *et al.*,[31] with the dashed grey line showing the extrapolation of the data reported by Wu *et al.* over the temperature range investigated in this work. The coral and light blue dashed lines are the parameterisations calculated by Lin *et al.*[38] and Long *et al.*,[41] respectively.

Fits to results for k' were performed over all relative humidities and temperatures studied in this work, with k_1, $k_{2,\mathrm{eff}}$ and $k_{3,\mathrm{eff}}$ described by Arrhenius expressions in which A and E_a were treated as global parameters for each reaction. However, the fits were insensitive to $k_{3,\mathrm{eff}}$, indicating that losses of CH_2OO owing to reaction with three water molecules were not significant under the conditions employed in this work. Subsequent fits to the data were performed to determine k_0, k_1, and $k_{2,\mathrm{eff}}$, with $k_{3,\mathrm{eff}}$ set to zero. Further details regarding analysis of the possible reaction involving three water molecules are given in the ESI.†

Fig. 3 shows the fit results for k', which gave $k_1 = (3.2 \pm 1.1) \times 10^{-13} \exp(-(2410 \pm 270)/T)$ cm^3 molecule^{-1} s^{-1} and $k_{2,\mathrm{eff}} = (2.78 \pm 0.28) \times 10^{-38} \exp((4010 \pm 400)/T)$cm^6 molecule^{-2} s^{-1}, where uncertainties represent a combination of the statistical error and the systematic errors resulting from uncertainties in relative humidity measurements and gas flow rates (see ESI†). Results for $k_{2,\mathrm{eff}}$ correspond to $k_2 = (2.85 \pm 0.40) \times 10^{-15} \exp((2417 \pm 338)/T)$ cm^3 molecule^{-1} s^{-1} using the temperature-dependent equilibrium constant for water dimer formation (K_{eq}^{D}), and associated uncertainties, reported by Ruscic *et al.*[51] The results are consistent with suggestions made in previous work[3,4,10,15,28,29] that the dominant loss of CH_2OO in the presence of water vapour occurs *via* reaction with water dimers (R2). No significant differences were obtained in results for kinetics of R2 between global fits over all conditions and local fits to kinetics at each temperature (see ESI†). The reaction of CH_2OO with water monomers (R1) was a minor contribution to the total loss of CH_2OO for all conditions employed in this work, with results for k_1 primarily defined by experiments performed at temperatures of 324 K and above. The kinetics of R1 were thus less well defined than those for R2, which represented the major contribution to the total CH_2OO loss at high relative humidities at all temperatures, and results for k_1 should be considered as estimates owing to the challenges associated with separating the impacts of k_0 and k_1.

Fig. 4 compares the results for k_1 obtained in this study with measurements, upper limits based on experimental observations, and theoretical calculations reported in previous work, with experimental results at ~298 K summarised in Table 1. Results for k_1 obtained in this work are systematically lower than those measured previously, but are consistent with the prediction of a positive barrier to reaction,[34–42] and are in agreement with calculated values of k_1 reported by Long *et al.*[43] at temperatures above 324 K, where results obtained in this work are more reliable. Previous direct experimental measurements of k_1 [15,27,31] at ~298 K, range between $(2.4 \pm 1.6) \times 10^{-16}$ cm^3 molecule^{-1} s^{-1} [15] and $(4.2 \pm 1.6) \times 10^{-16}$ cm^3 molecule^{-1} s^{-1},[31] compared to the value of $(9.8 \pm 5.9) \times 10^{-17}$ cm^3

Table 1 Comparison between k_1 values obtained at room temperature in this work and in previous literature.[5,10,15,18,27,28,31] LFP = laser flash photolysis, PIMS = photoionisation mass spectrometry, CI-APi-TOF-MS = chemical ionisation-atmospheric pressure interface-time-of-flight mass spectrometry, UV abs = ultraviolet absorption, RR = relative rate study. The k_1 value in the base model described in the Atmospheric implications section was 1.7×10^{-15} cm^3 molecule^{-1} s^{-1} at 298 K [13] and the k_1 value in the first set of model updates was 2.8×10^{-16} cm^3 molecule^{-1} s^{-1} at 298 K [30]

T/K	p/Torr	Experimental technique	$k_1/10^{-17}$ cm^3 molecule^{-1} s^{-1}	Reference
298	4	LFP/PIMS	≤400	Welz *et al.*[18]
295	200	LFP/LIF	≤9	Stone *et al.*[5]
297	760	Ozonolysis/CI-APi-TOF-MS	32 ± 12	Berndt *et al.*[27]
298	50–400	LFP/UV abs	≤150	Chao *et al.*[28]
298	760	RR. Ethene ozonolysis	130 ± 40	Newland *et al.*[10]
293	30–100	LFP/UV abs	24 ± 16	Sheps *et al.*[15]
298	300	LFP/UV abs	42 ± 5	Wu *et al.*[31]
298	760	LFP/UV abs	9.8 ± 5.9	This work

molecule^{-1} s^{-1} indicated in this work. Theory predicts values between 5.8 × 10^{-18} cm^3 molecule^{-1} s^{-1} [34] and 7.08 × 10^{-15} cm^3 molecule^{-1} s^{-1},[44] with the most recent theoretical study giving k_1 = 7.08 × 10^{-15} cm^3 molecule^{-1} s^{-1}.[43] The temperature dependence for k_1 indicated in this work is more significant than the temperature dependence reported by Wu *et al.*[31]

Whilst there are significant uncertainties in k_1, the kinetics of R2 are well-defined from the fits shown in Fig. 3. Fig. 5 shows the temperature dependence of $k_{2,\mathrm{eff}}$, which is in good agreement with previous measurements[3,28,50] over the temperature ranges in common, with this work extending the temperature range over which the kinetics have been investigated. At 298 K, this work indicates $k_{2,\mathrm{eff}} = (1.96 \pm 0.51) \times 10^{-32}$ cm^6 molecule^{-2} s^{-1}, which corresponds to $k_2 = (9.5 \pm 2.5) \times 10^{-12}$ cm^3 molecule^{-1} s^{-1} using the temperature-dependent equilibrium constant for water dimer formation reported by Ruscic *et al.*[51] Table 2 compares results for k_2 and $k_{2,\mathrm{eff}}$ obtained at 298 K in this work with those reported previously, with good agreement between the results reported here and the results of Berndt *et al.*,[3] Smith *et al.*,[29] Chao *et al.*[28] and Sheps *et al.*[15] The value for $k_{2,\mathrm{eff}}$ reported by Wu *et al.*[31] at 298 K is a factor of ~1.8 lower than that reported here, but there is good agreement in the total pseudo-first-order rate coefficients as a function of water monomer concentration observed in this work and reported by Wu *et al.* (see ESI† for further details). Although Wu *et al.*[31] reported an impact of a reaction between CH_2OO and three water molecules, it was noted that there was little impact of the reaction involving three water molecules for water monomer concentrations below 4.8 × 10^{17} molecule cm^{-3} at 298 K, which is higher than the highest water concentrations used in this work at 298 K. The differences in kinetics for R2 between the results of Wu *et al.* and other studies, including this work, are impacted by differences in kinetics for R1 as well as contributions from R3, making direct comparison of rate coefficients for individual reactions difficult. Rate coefficients reported by Newland *et al.*[10] for R2 at 298 K are notably lower than those reported elsewhere, but these experiments were carried out over a relatively narrow range of relative humidities (1.5 to 20%), leading to low water dimer concentrations and relatively limited impact of the dimer reaction. Lewis *et al.*[4] also reported lower values than those obtained in this work and in other studies using flash photolysis with UV absorption,[15,28,29] potentially resulting from overestimation of the water vapour, and thus water dimer, concentrations, which were based on flow rates and vapour pressure and assumed 100% saturation of the gas flow with water vapour. Results reported here, and in other studies using flash photolysis with UV absorption,[28,29,31] measured the relative humidity of the gas flow, providing greater certainty in the water vapour and dimer concentrations.

The temperature-dependent behaviour observed for $k_{2,\mathrm{eff}}$ is in agreement with previous experimental[29,31] and theoretical[34,35]

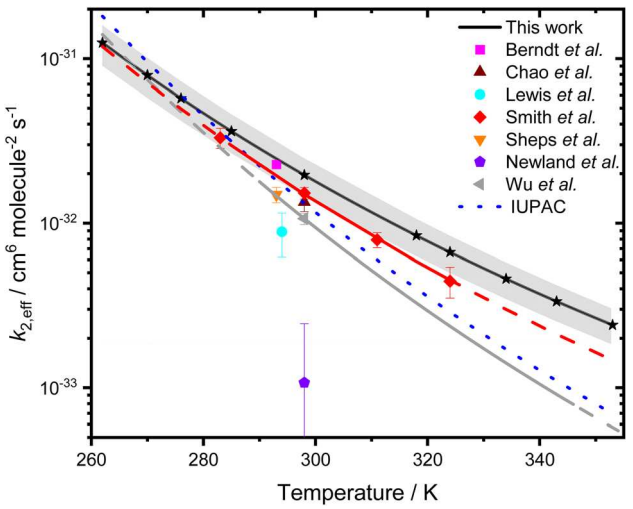

Fig. 5 $k_{2,\mathrm{eff}}$ as a function of temperature. The global fit to results obtained in this work is shown by the solid black line, with uncertainties determined from a combination of the statistical error and the systematic errors resulting from uncertainties in gas flow rates and in the concentration of [H_2O] shown by the shaded region. Stars represent the temperatures at which measurements were made. The solid grey line shows the data reported by Wu *et al.*,[31] with the dashed grey line showing the extrapolation of the data reported by Wu *et al.* over the temperature range investigated in this work. The red solid line represents a fit to the data reported by Smith *et al.*,[50] with the dashed red line showing the extrapolation of the data reported by Smith *et al.* over the temperature range investigated in this work. The blue dotted line represents the current IUPAC recommendation,[30] which is based on the data reported by Smith *et al.*

Table 2 Comparison between the k_2 values obtained at room temperature in this work and in previous literature.[3,4,10,15,28,29,31] LFP = laser flash photolysis, UV abs = ultraviolet absorption, IfT-LFT = Institute for Tropospheric Research – Laminar Flow Tube, RR = relative rate study. $k_{2,\mathrm{eff}}$ values have been calculated using the K_{eq}^{D} values reported by Ruscic *et al.*[51] The k_2 value in the base model described in the Atmospheric implications section was 1.5 × 10^{-12} cm^3 molecule^{-1} s^{-1} at 298 K[13] and the k_2 value in the first set of model updates was 6.4 × 10^{-12} cm^3 molecule^{-1} s^{-1} at 298 K[30]

T/K	p/Torr	Experimental technique	k_2/10^{-12} cm^3 molecule^{-1} s^{-1}	$k_{2,\mathrm{eff}}$/10^{-32} cm^6 molecule^{-2} s^{-1}	Reference
293	760	IfT-LFT (H_2SO_4) measurements	10.7 ± 0.40	2.28 ± 0.09	Berndt *et al.*[3]
298	100–500	LFP/UV abs	6.5 ± 0.8	1.34 ± 0.17	Chao *et al.*[28]
294	50–400	LFP/UV abs	4.0 ± 1.2	0.89 ± 0.27	Lewis *et al.*[4]
298	200–600	LFP/UV abs	7.4 ± 0.6	1.53 ± 0.12	Smith *et al.*[29]
293	30–100	LFP/UV abs	6.6 ± 0.7	1.49 ± 0.16	Sheps *et al.*[15]
298	760	RR. Ethene ozonolysis	0.52 ± 0.67	0.11 ± 0.14	Newland *et al.*[10]
298	300	LFP/UV abs	5.17 ± 0.40	1.07 ± 0.08	Wu *et al.*[31]
298	760	LFP/UV abs	9.52 ± 2.49	1.96 ± 0.51	This work

Table 3 Previous theoretical calculations of the potential energy surface for R1 and R2 and, where available, calculations of the reaction kinetics. Where multiple reaction pathways for R1 and R2 were given, the lowest energy pathway was chosen. PRC = pre-reaction complex, TS = transition state, CTST = conventional transition state theory, VTST = variational transition state theory, VPT2 = vibrational second-order perturbation theory, MP-CVT/SCT = multipath variational transition state theory with small-curvature tunneling, CUS = canonical unified statistical theory

Method	PRC R1/kJ mol^{-1}	TS R1/kJ mol^{-1}	PRC R2/kJ mol^{-1}	TS R2/kJ mol^{-1}	k_1/cm^3 molecule^{-1} s^{-1}	k_2/cm^3 molecule^{-1} s^{-1}	Ref.
CCSD(T)/6-311G(d,p)	−30.1	9.6	—	—	—	—	39
CCSD(T)/6-311+G(2d,2p)	−32.6	7.9	—	—	—	—	40
CCSD(T)/6-311+G(2d,2p) CTST	−30.9	14.2	−65.7	−36.8	5.8×10^{-18}	1.1×10^{-12}	34
CCSD(T)/aug-cc-pVTZ C/VTST	−26.0	8.5	—	—	3.12×10^{-15}	—	36
W3X-L//CCSD(T)-F12a/TZ-F12 MP-CVT/SCT	−26.2	14.7	—	—	2.41×10^{-16}	—	41
CCSD(T)/aug-cc-PVTZ VTST	−25.7	6.3	−44.8	−35.5	3.05×10^{-15}	1.67×10^{-10}	35
CCSD(T)//M06-2X/6-311+G(2d,2p) CTST	−28.5	11.2	−63.7	−45.3	—	6.71×10^{-12}	42
QCISD(T)/CBS//6-311+G(2d,2p) VPT2	−27.3	11.8	−46.2	−27.3	3.7×10^{-16}	5.4×10^{-12}	38
B3LYP/6-311+G(2d,2p) VPT2	−26.4	12.8	−42.4	−24.6	4.26×10^{-16}	2.91×10^{-12}	37
CCSD(T)/6-311+G(3df,2dp) CTST	−25.9	14.2	−32.0	−8.4	7.08×10^{-15}	1.15×10^{-12}	44
W3X-L//CCSD(T)- F12a/cc-pVDZ-F12[a] W3X-L//CCSD(T)-F12a/cc-pVTZ-F12[b] CUS	—	—	−45.5	−22.9	—	6.73×10^{-12}	43

[a] Level of theory used to optimise geometries and energies for reactant, PRCs, and products. [b] Level of theory used to optimise geometries and energies for the transition states.

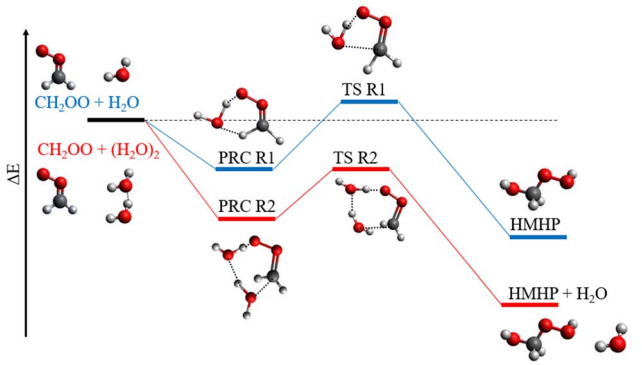

Fig. 6 Schematic potential energy surface for the reactions of CH_2OO with H_2O (blue) and $(H_2O)_2$ (red). PRC = pre-reaction complex, TS = transition state, HMHP = hydroxymethyl hydroperoxide.

work. Rate coefficients obtained in this work are in agreement with those reported by Smith *et al.* and Wu *et al.* over the common temperature ranges, but there are some discrepancies between the measurements made at the highest temperature employed in this work, and extrapolation of the results reported by Smith *et al.* and Wu *et al.*,[31] as shown in Fig. 5. Observations of a negative temperature dependence for the kinetics of R2, and of the dominance of R2 over R1, are consistent with theoretical studies of R1 and R2.[34,35,37,38] Calculations of the potential energy surfaces for R1 and R2, summarised in Table 3 and Fig. 6,[34–43] indicate that both reactions proceed *via* the formation of pre-reaction complexes which then undergo rearrangement to form HMHP as the dominant product of both reactions, although experimental work has indicated that there may be other reaction channels or rapid subsequent chemistry of the HMHP product leading to the production of species including HCOOH, HCHO and H_2O_2. For R1, rearrangement of the pre-reaction complex to HMHP involves a transition state which is higher in energy than the initial reactants (*i.e.* there is an overall positive barrier to reaction). In contrast, the pre-reaction complex for R2 is more stable than that for R1 by a factor of ~2 (Table 3 and Fig. 6), and the subsequent transition state to product formation is lower in energy than the initial reactants. The difference in barrier heights leads to the dominance of R2 over R1, and the submerged barrier for R2 leads to the observed negative temperature dependence.

Atmospheric implications

The reaction of CH_2OO with water dimers is expected to dominate the atmospheric chemistry of CH_2OO.[3,15,28,29] Model simulations were performed with the global 3D atmospheric chemistry transport model (CTM) GEOS-Chem (version 14.2.2 [52]) to assess the impact of this work on our understanding of CH_2OO in the atmosphere. The model was run for 2 years (2018–2019) driven by MERRA-2 meteorology[53] with a 4.0° × 4.5° spatial resolution and 72 vertical levels. The first year was considered as model spin up and discarded. The model contains detailed VOC oxidation chemistry[54] including Criegee intermediate reactions.[14] Biogenic emissions of VOCs were

Table 4 Summary of reactions, products, rate coefficients and percentage losses for CH_2OO reactions used in the three model simulations described in the atmospheric implications section of this work

Reaction	Products	Base model		First set of updates		Second set of updates	
		Rate coefficient/ cm^3 $molecule^{-1}$ s^{-1} (second-order reactions) or cm^6 $molecule^{-2}$ s^{-1} (third-order reactions)	Loss/%	Rate coefficient/ cm^3 $molecule^{-1}$ s^{-1} (second-order reactions) or cm^6 $molecule^{-2}$ s^{-1} (third-order reactions)	Loss/%	Rate coefficient/ cm^3 $molecule^{-1}$ s^{-1} (second-order reactions) or cm^6 $molecule^{-2}$ s^{-1} (third-order reactions)	Loss/%
$CH_2OO + H_2O$	0.73 HMHP + 0.21 HCOOH + 0.21 H_2O + 0.06 HCHO + 0.06 H_2O_2	$1.7 \times 10^{-15\ 13}$	64.74	$2.8 \times 10^{-16\ 30}$	3.77	3.2×10^{-13} exp(−2410/T)	0.82
$CH_2OO + H_2O + H_2O$	0.40 HMHP + 0.54 HCOOH + 0.54 H_2O + 0.06 HCHO + 0.06 H_2O_2	$2.88 \times 10^{-35} \times \exp(1319/T)^{13}$	32.45	$7.35 \times 10^{-18} \times \exp(4076/T)^{30}$	96.03	2.78×10^{-38} exp(4010/T)	98.32
$CH_2OO + O_3$	HCHO + $2O_2$	$1.4 \times 10^{-12\ 59}$	0.03	$3.60 \times 10^{-13\ 60}$	0.01	$3.60 \times 10^{-13\ 21}$	0.03
$CH_2OO + SO_2$	HCHO + SO_3	$3.70 \times 10^{-11\ 59}$	2.79	$3.72 \times 10^{-11} \times (T/298)^{-2.05\ 20}$	0.19	$3.72 \times 10^{-11} \times (T/298)^{-2.05\ 20}$	0.83
$CH_2OO + NO_2$	HCHO + NO_3	$1.00 \times 10^{-15\ 14}$	<0.01	$3.00 \times 10^{-12\ 30}$	<0.01	$3.00 \times 10^{-12\ 30}$	<0.01
$CH_2OO + NO$	HCHO + NO_2	$1.00 \times 10^{-14\ 14}$	<0.01	—	—	—	—
$CH_2OO + CO$	HCHO + CO_2	$1.20 \times 10^{-15\ 14}$	0.01	—	—	—	—

taken from MEGANv2.1,[55] biomass burning emissions from GFED4s,[56] while anthropogenic emissions use the Community Emissions Data System (CEDS).[57]

The Criegee intermediate chemistry in the base model was described in 2015 [58] and subsequently updated by Bates *et al.*[54] in 2021 to the current CH_2OO chemistry in the base model shown in Table 4. Model runs in this work have been performed with the base chemistry and then with two sets of updates. The first update represents the state of current understanding, and involves updates to the rate coefficients for the reactions of CH_2OO with H_2O, $(H_2O)_2$, and NO_2 to the values currently recommended by IUPAC,[30] and to the rate coefficients of reactions with O_3 and SO_2 to the values reported in our previous work.[20,21] In the first update we have also removed the reactions of CH_2OO with NO or CO as the kinetics of these reactions are highly uncertain, and the reactions are not expected to represent significant losses for CH_2OO. The second update to the model changes the rate coefficient for reactions R1 and R2 from those currently recommended by IUPAC to those determined in the experiments described in this work. The complete set of CH_2OO chemistry used in the model is described in Table 4. Comparisons between the temperature-dependent rate coefficients for $CH_2OO + H_2O$ and $CH_2OO + (H_2O)_2$ in the three model simulations are given in the ESI (Fig. S8†). Kinetics for the reaction of CH_2OO with water vapour in the base GEOS-Chem mechanism were estimated from the relative rates of CH_2OO reactions with SO_2 and water monomers, with a temperature dependence estimated from the temperature dependence of the equilibrium between water monomers and dimers, as described in previous work.[13,54,61] Rate coefficients for R2 measured in this work are typically two orders of magnitude greater than those estimated in the simulations for the base case, leading to significant changes in the behaviour of CH_2OO in the model.

Fig. 7 shows the impact of the changes made in the first update, compared to the base model run, on annual mean surface layer concentrations for CH_2OO and several key atmospheric species. The model shows significant decreases in CH_2OO in most locations, with mean surface layer concentrations decreased by 64.2% compared to the base model run owing to the faster kinetics for $CH_2OO + (H_2O)_2$ used in the updated model. However, there are some regional differences to the global mean trend, with hot and dry regions over areas including Australia and parts of Africa and the Middle East displaying significant increases in the concentration of CH_2OO. In these regions, the impacts of updates to $k_{2,eff}$ are limited as a result of low water dimer concentrations owing to low water monomer concentrations and the temperature dependence of the equilibrium between H_2O and $(H_2O)_2$, with the observed impact dominated by the decreased values for k_1 used in the updated model.

The first set of model updates also affect concentrations of products formed in CH_2OO reactions with H_2O and $(H_2O)_2$, which are based on the work of Nguyen *et al.*[13] and thus consider the yields of products on longer timescales than the initial production of HMHP from the elementary reactions R1 and R2. In the first set of model updates, the annual mean surface layer concentration for HCOOH is increased by 10.1%, while that for HMHP is decreased by 33.7% owing to an increase in importance of the dimer reaction, which favours production of HCOOH over HMHP. Concentrations of other key

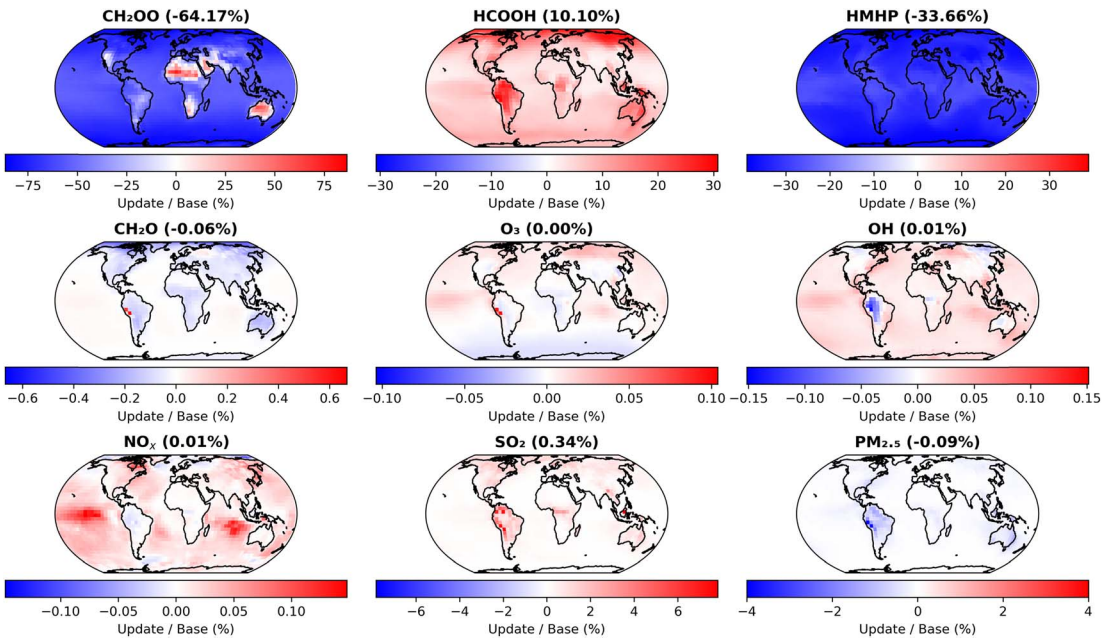

Fig. 7 Impacts of changes made in the first set of GEOS-Chem updates (Table 4, 'First set of updates'), compared to the base model run (Table 4, 'Base model'), on annual mean surface layer mixing ratios for CH_2OO and several key atmospheric species. The first set of model updates incorporate current IUPAC recommendations for k_1 and $k_{2,eff}$, as well as updates to rate coefficients for reactions of CH_2OO with O_3, SO_2, and NO_2.

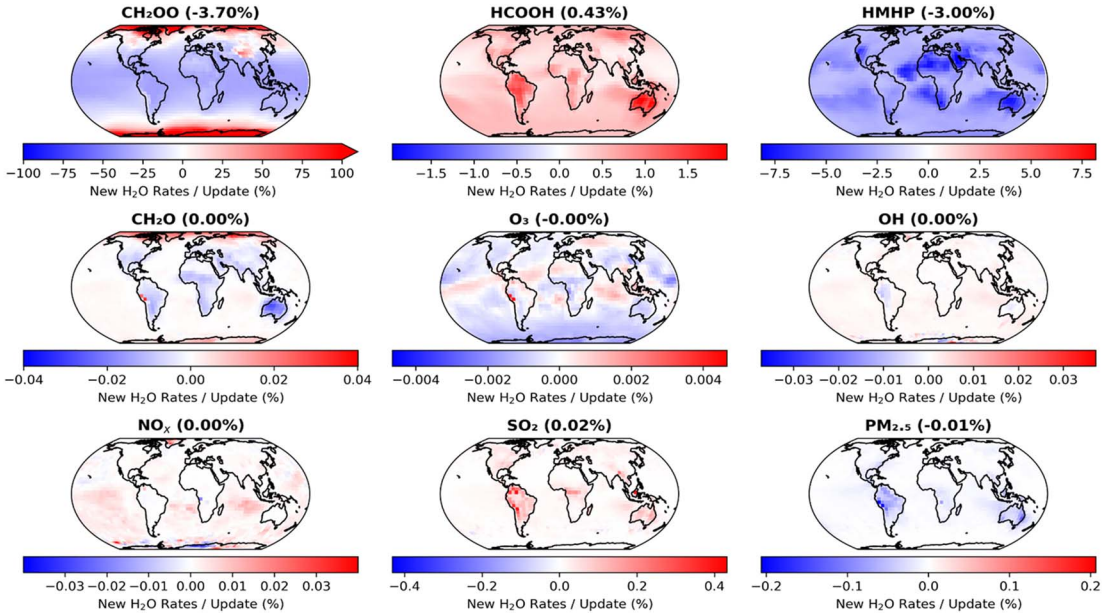

Fig. 8 Impacts of changes made in the second set of GEOS-Chem updates (Table 4, 'Second set of updates'), compared to the results obtained with the first set of updates (Table 4, 'First set of updates'), on annual mean surface layer mixing ratios for CH_2OO and several key atmospheric species. The second set of model updates make use of the results obtained in this work for k_1 and $k_{2,eff}$.

atmospheric species display smaller changes, with SO_2 showing regional surface layer increases of over 6% but an overall annual mean surface layer change of 0.3%, and $PM_{2.5}$ (particulate matter of less than 2.5 μm diameter) showing decreases of up to 4% regionally but with a decrease in the overall annual mean surface layer of 0.1%.

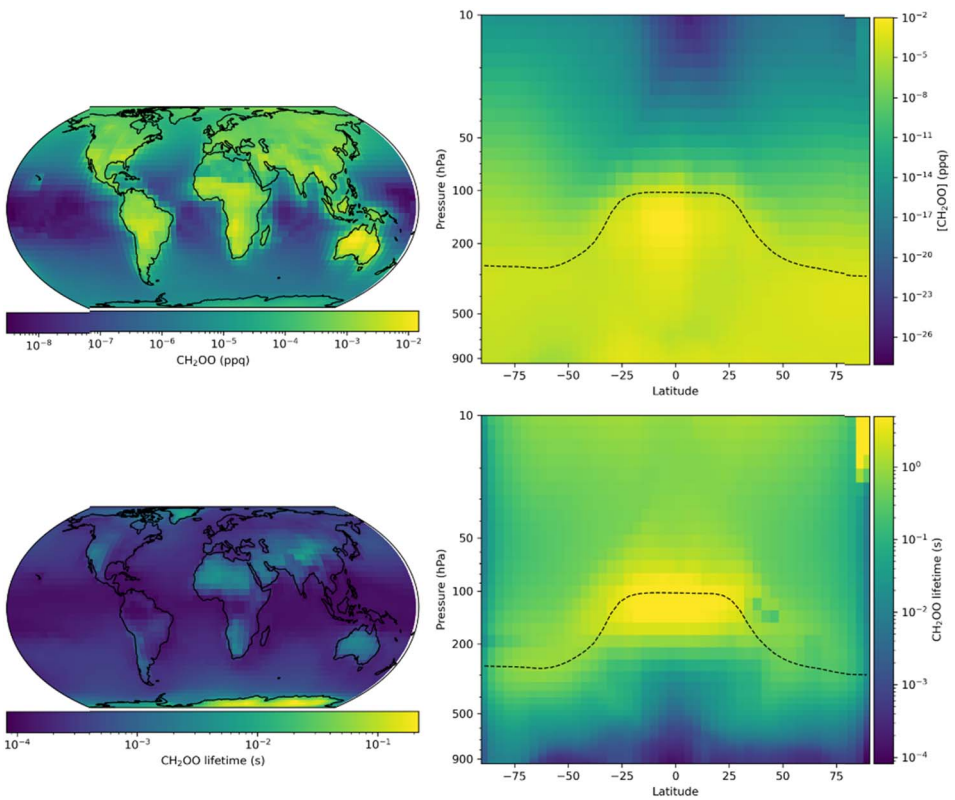

Fig. 9 Annual mean CH_2OO surface layer mixing ratios and zonal distributions (top panel) and lifetime (bottom panel) for GEOS-Chem simulations using the second set of model updates, which make used of results obtained in this work for k_1 and $k_{2,eff}$ (Table 4, 'Second set of updates').

The impacts of the second set of model updates, which make use of the results obtained in this work, are shown in Fig. 8. Further decreases in CH_2OO concentrations are observed, with a reduction in the annual mean surface layer concentration of 3.7% compared to that obtained in the model run using the first set of updates, with little regional variation, and 61.8% compared to the base model run. However, changes to other species are more limited, with an increase in HCOOH of only 0.4% and a decrease in HMHP of only 3.0% compared to the overall annual mean surface concentrations obtained in the model run using the first set of updates. Species such as SO_2 and $PM_{2.5}$ display little difference compared to the results obtained with the first set of model updates.

Fig. 9 shows annual mean surface layer mixing ratios of CH_2OO obtained for the model run updated with results obtained in this work. The annual surface layer mixing ratio of CH_2OO peaks at 1.5×10^{-2} ppq, which is equivalent to a number density of 3.7×10^2 molecule cm^{-3} at 298 K and 760 Torr, with an annual mean of 3.5×10^{-4} ppq. Mixing ratios of CH_2OO are highest over landmasses where the emissions of unsaturated VOCs into the atmosphere are highest, and lowest over remote oceanic regions. Vertically, the highest mixing ratios (1.9×10^{-2} ppq) are seen in the tropical upper troposphere, where convective lifting brings unsaturated VOCs into contact with high O_3 concentrations in a region with low concentrations of water vapour. The mean lifetime of CH_2OO in the updated model is 0.45 s, reaching a minimum of 9.8×10^{-4} s in the marine surface layer and a maximum of >2 s in the upper troposphere owing to low water concentrations. In the updated model, the tropospheric annual mean global loss of CH_2OO is dominated by the reaction with water dimers, which represents 98.3% of the total CH_2OO loss, with a further 0.8% of the total loss occurring through reaction with water monomers. Reactions of CH_2OO with species other than water account for less than 1% of the total loss, other than in a few regions, primarily northern Eurasia, where this reaches up to 4%. The updated simulations restrict the importance of non-water reactions significantly, although there may be more localised impacts which are not realised in this work owing to the spatial resolution of the simulations.

Conclusions

The kinetics of the reaction of the simplest Criegee intermediate, CH_2OO, with water vapour have been investigated using laser flash photolysis coupled with time-resolved broadband UV absorption spectroscopy at temperatures between 262 and 353 K at a total pressure of 760 Torr. The reaction of CH_2OO with water monomers (R1) represents a minor contribution to the total loss of CH_2OO under the conditions employed in this work, with an estimated value for k_1 of $(9.8 \pm 5.9) \times 10^{-17}$ cm^3 $molecule^{-1}$ s^{-1} at 298 K and a temperature dependence described by $k_1 = (3.2 \pm 1.1) \times 10^{-13} \exp(-(2410 \pm 270)/T)$ cm^3 $molecule^{-1}$ s^{-1}. The results show that the reaction with water dimers (R2) dominates the loss of CH_2OO, with $k_2 = (9.5 \pm 2.5) \times 10^{-12}$ cm^3 $molecule^{-1}$ s^{-1} at 298 K, with a temperature dependence described by $k_2 = (2.85 \pm 0.40) \times 10^{-15} \exp((2420 \pm 340)/T)$ cm^3 $molecule^{-1}$ s^{-1}, where use of k_2 requires calculation of the water dimer concentration to determine the rate of reaction. The kinetics of R2 can also be expressed in terms of an effective rate coefficient, $k_{2,eff}$, which is given by the product $k_2K_{eq}^D$, allowing calculation of the rate of reaction in terms of the square of the water monomer concentration rather than the water dimer concentration, giving $k_{2,eff} = (1.96 \pm 0.51) \times 10^{-32}$ cm^6 $molecule^{-2}$ s^{-1} at 298 K and a temperature dependence described by $k_{2,eff} = (2.78 \pm 0.28) \times 10^{-38} \exp((4010 \pm 400)/T)$ cm^6 $molecule^{-2}$ s^{-1}. No significant impact of a reaction between CH_2OO and three water molecules was observed in this work. The kinetic results are consistent with theoretical studies which predict the existence of a positive barrier to reaction for R1 and a submerged barrier for R2. Simulations performed using the global CTM GEOS-Chem updated with the experimental results obtained in this work indicate that the reaction of CH_2OO with water dimers is expected to dominate the atmospheric chemistry of CH_2OO, limiting the impacts of reactions of CH_2OO with other species. Uncertainties in the product yields of CH_2OO reactions with water monomers and dimers remain, which limit our understanding of the atmospheric impacts of CH_2OO chemistry.

Data availability

Relevant data supporting this article have been included as part of the ESI.†

Conflicts of interest

There are no conflicts to declare.

Acknowledgements

The authors thank the Natural Environment Research Council (NERC) for funding (grant reference NE/P012876/1).

References

1 D. Johnson and G. Marston, The gas-phase ozonolysis of unsaturated volatile organic compounds in the troposphere, *Chem. Soc. Rev.*, 2008, **37**(4), 699–716.
2 D. Stone, K. Au, S. Sime, D. J. Medeiros, M. Blitz, P. W. Seakins, Z. Decker and L. Sheps, Unimolecular decomposition kinetics of the stabilised Criegee intermediates CH_2OO and CD_2OO, *Phys. Chem. Chem. Phys.*, 2018, **20**(38), 24940–24954.
3 T. Berndt, J. Voigtländer, F. Stratmann, H. Junninen, R. L. Mauldin III, M. Sipilä, M. Kulmala and H. Herrmann, Competing atmospheric reactions of CH_2OO with SO_2 and water vapour, *Phys. Chem. Chem. Phys.*, 2014, **16**(36), 19130–19136.
4 T. R. Lewis, M. A. Blitz, D. E. Heard and P. W. Seakins, Direct evidence for a substantive reaction between the Criegee intermediate, CH_2OO, and the water vapour dimer, *Phys. Chem. Chem. Phys.*, 2015, **17**(7), 4859–4863.

5 D. Stone, M. Blitz, L. Daubney, N. U. M. Howes and P. Seakins, Kinetics of CH_2OO reactions with SO_2, NO_2, NO, H_2O and CH_3CHO as a function of pressure, *Phys. Chem. Chem. Phys.*, 2014, **16**(3), 1139–1149.

6 N. U. M. Howes, Z. S. Mir, M. A. Blitz, S. Hardman, T. R. Lewis, D. Stone and P. W. Seakins, Kinetic studies of C1 and C2 Criegee intermediates with SO_2 using laser flash photolysis coupled with photoionization mass spectrometry and time resolved UV absorption spectroscopy, *Phys. Chem. Chem. Phys.*, 2018, **20**(34), 22218–22227.

7 M. Suto, E. R. Manzanares and L. C. Lee, Detection of sulfuric acid aerosols by ultraviolet scattering, *Environ. Sci. Technol.*, 1985, **19**(9), 815–820.

8 K. H. Becker, J. Bechara and K. J. Brockmann, Studies on the formation of H_2O_2 in the ozonolysis of alkenes, *Atmos. Environ., Part A*, 1993, **27**(1), 57–61.

9 K. E. Leather, M. R. McGillen, M. C. Cooke, S. R. Utembe, A. T. Archibald, M. E. Jenkin, R. G. Derwent, D. E. Shallcross and C. J. Percival, Acid-yield measurements of the gas-phase ozonolysis of ethene as a function of humidity using Chemical Ionisation Mass Spectrometry (CIMS), *Atmos. Chem. Phys.*, 2012, **12**(1), 469–479.

10 M. J. Newland, A. R. Rickard, M. S. Alam, L. Vereecken, A. Muñoz, M. Ródenas and W. J. Bloss, Kinetics of stabilised Criegee intermediates derived from alkene ozonolysis: reactions with SO_2, H_2O and decomposition under boundary layer conditions, *Phys. Chem. Chem. Phys.*, 2015, **17**(6), 4076–4088.

11 A. S. Hasson, G. Orzechowska and S. E. Paulson, Production of stabilized Criegee intermediates and peroxides in the gas phase ozonolysis of alkenes: 1. Ethene, trans-2-butene, and 2,3-dimethyl-2-butene, *J. Geophys. Res.: Atmos.*, 2001, **106**(D24), 34131–34142.

12 G. E. Orzechowska and S. E. Paulson, Photochemical Sources of Organic Acids. 1. Reaction of Ozone with Isoprene, Propene, and 2-Butenes under Dry and Humid Conditions Using SPME, *J. Phys. Chem. A*, 2005, **109**(24), 5358–5365.

13 T. B. Nguyen, G. S. Tyndall, J. D. Crounse, A. P. Teng, K. H. Bates, R. H. Schwantes, M. M. Coggon, L. Zhang, P. Feiner, D. O. Milller, K. M. Skog, J. C. Rivera-Rios, M. Dorris, K. F. Olson, A. Koss, R. J. Wild, S. S. Brown, A. H. Goldstein, J. A. de Gouw, W. H. Brune, F. N. Keutsch, J. H. Seinfeld and P. O. Wennberg, Atmospheric fates of Criegee intermediates in the ozonolysis of isoprene, *Phys. Chem. Chem. Phys.*, 2016, **18**(15), 10241–10254.

14 D. B. Millet, M. Baasandorj, D. K. Farmer, J. A. Thornton, K. Baumann, P. Brophy, S. Chaliyakunnel, J. A. de Gouw, M. Graus, L. Hu, A. Koss, B. H. Lee, F. D. Lopez-Hilfiker, J. A. Neuman, F. Paulot, J. Peischl, I. B. Pollack, T. B. Ryerson, C. Warneke, B. J. Williams and J. Xu, A large and ubiquitous source of atmospheric formic acid, *Atmos. Chem. Phys.*, 2015, **15**(11), 6283–6304.

15 L. Sheps, B. Rotavera, A. J. Eskola, D. L. Osborn, C. A. Taatjes, K. Au, D. E. Shallcross, M. A. H. Khan and C. J. Percival, The reaction of Criegee intermediate CH_2OO with water dimer: primary products and atmospheric impact, *Phys. Chem. Chem. Phys.*, 2017, **19**(33), 21970–21979.

16 C. A. Taatjes, O. Welz, A. J. Eskola, J. D. Savee, A. M. Scheer, D. E. Shallcross, B. Rotavera, E. P. F. Lee, J. M. Dyke, D. K. W. Mok, D. L. Osborn and C. J. Percival, Direct Measurements of Conformer-Dependent Reactivity of the Criegee Intermediate CH_3CHOO, *Science*, 2013, **340**(6129), 177.

17 H.-L. Huang, W. Chao and J. J.-M. Lin, Kinetics of a Criegee intermediate that would survive high humidity and may oxidize atmospheric SO_2, *Proc. Natl. Acad. Sci. U. S. A.*, 2015, **112**(35), 10857–10862.

18 O. Welz, J. D. Savee, D. L. Osborn, S. S. Vasu, C. J. Percival, D. E. Shallcross and C. A. Taatjes, Direct Kinetic Measurements of Criegee Intermediate (CH_2OO) Formed by Reaction of CH_2I with O_2, *Science*, 2012, **335**(6065), 204.

19 J. Peltola, P. Seal, A. Inkila and A. J. Eskola, Time-resolved, broadband UV-absorption spectrometry measurements of Criegee intermediate kinetics using a new photolytic precursor: unimolecular decomposition of CH_2OO and its reaction with formic acid, *Phys. Chem. Chem. Phys.*, 2020, **22**, 11797–11808.

20 L. Onel, R. Lade, J. Mortiboy, M. A. Blitz, P. W. Seakins, D. E. Heard and D. Stone, Kinetics of the gas phase reaction of the Criegee intermediate CH_2OO with SO_2 as a function of temperature, *Phys. Chem. Chem. Phys.*, 2021, **23**(35), 19415–19423.

21 Z. S. Mir, T. R. Lewis, L. Onel, M. A. Blitz, P. W. Seakins and D. Stone, CH_2OO Criegee intermediate UV absorption cross-sections and kinetics of CH_2OO + CH_2OO and CH_2OO + I as a function of pressure, *Phys. Chem. Chem. Phys.*, 2020, **22**(17), 9448–9459.

22 B. Ouyang, M. W. McLeod, R. L. Jones and W. J. Bloss, NO_3 radical production from the reaction between the Criegee intermediate CH_2OO and NO_2, *Phys. Chem. Chem. Phys.*, 2013, **15**(40), 17070–17075.

23 R. L. Caravan, M. A. H. Khan, B. Rotavera, E. Papajak, I. O. Antonov, M.-W. Chen, K. Au, W. Chao, D. L. Osborn, J. J.-M. Lin, C. J. Percival, D. E. Shallcross and C. A. Taatjes, Products of Criegee intermediate reactions with NO_2: experimental measurements and tropospheric implications, *Faraday Discuss.*, 2017, **200**, 313–330.

24 L. Vereecken, H. Harder and A. Novelli, The reaction of Criegee intermediates with NO, RO_2, and SO_2, and their fate in the atmosphere, *Phys. Chem. Chem. Phys.*, 2012, **14**(42), 14682–14695.

25 K. T. Kuwata, E. J. Guinn, M. R. Hermes, J. A. Fernandez, J. M. Mathison and K. Huang, A Computational Re-examination of the Criegee Intermediate–Sulfur Dioxide Reaction, *J. Phys. Chem. A*, 2015, **119**(41), 10316–10335.

26 Y.-Y. Wang, M. R. Dash, C.-Y. Chung and Y.-P. Lee, Detection of transient infrared absorption of SO_3 and 1,3,2-dioxathietane-2,2-dioxide [cyc-$(CH_2)O(SO_2)O$] in the reaction CH_2OO+SO_2, *J. Chem. Phys.*, 2018, **148**(6), 064301.

27 T. Berndt, R. Kaethner, J. Voigtländer, F. Stratmann, M. Pfeifle, P. Reichle, M. Sipilä, M. Kulmala and M. Olzmann, Kinetics of the unimolecular reaction of

CH_2OO and the bimolecular reactions with the water monomer, acetaldehyde and acetone under atmospheric conditions, *Phys. Chem. Chem. Phys.*, 2015, **17**(30), 19862–19873.

28 W. Chao, J.-T. Hsieh, C.-H. Chang and J. J.-M. Lin, Direct kinetic measurement of the reaction of the simplest Criegee intermediate with water vapor, *Science*, 2015, **347**(6223), 751.

29 M. C. Smith, C.-H. Chang, W. Chao, L.-C. Lin, K. Takahashi, K. A. Boering and J. J.-M. Lin, Strong Negative Temperature Dependence of the Simplest Criegee Intermediate CH_2OO Reaction with Water Dimer, *J. Phys. Chem. Lett.*, 2015, **6**(14), 2708–2713.

30 R. A. Cox, M. Ammann, J. N. Crowley, H. Herrmann, M. E. Jenkin, V. F. McNeill, A. Mellouki, J. Troe and T. J. Wallington, Evaluated kinetic and photochemical data for atmospheric chemistry: Volume VII – Criegee intermediates, *Atmos. Chem. Phys.*, 2020, **20**(21), 13497–13519.

31 Y.-J. Wu, K. Takahashi and J. J.-M. Lin, Kinetics of the Simplest Criegee Intermediate Reaction with Water Vapor: Revisit and Isotope Effect, *J. Phys. Chem. A*, 2023, **127**(39), 8059–8072.

32 K. H. Becker, K. J. Brockmann and J. Bechara, Production of hydrogen peroxide in forest air by reaction of ozone with terpenes, *Nature*, 1990, **346**(6281), 256–258.

33 M. Nakajima and Y. Endo, Observation of hydroxymethyl hydroperoxide in a reaction system containing CH_2OO and water vapor through pure rotational spectroscopy, *J. Chem. Phys.*, 2015, **143**(16), 164307.

34 A. B. Ryzhkov and P. A. Ariya, A theoretical study of the reactions of parent and substituted Criegee intermediates with water and the water dimer, *Phys. Chem. Chem. Phys.*, 2004, **6**(21), 5042–5050.

35 J. M. Anglada and A. Solé, Impact of the water dimer on the atmospheric reactivity of carbonyl oxides, *Phys. Chem. Chem. Phys.*, 2016, **18**(26), 17698–17712.

36 J. M. Anglada, J. González and M. Torrent-Sucarrat, Effects of the substituents on the reactivity of carbonyl oxides. A theoretical study on the reaction of substituted carbonyl oxides with water, *Phys. Chem. Chem. Phys.*, 2011, **13**(28), 13034–13045.

37 C. Yin and K. Takahashi, Effect of unsaturated substituents in the reaction of Criegee intermediates with water vapor, *Phys. Chem. Chem. Phys.*, 2018, **20**(30), 20217–20227.

38 L.-C. Lin, H.-T. Chang, C.-H. Chang, W. Chao, M. C. Smith, C.-H. Chang, J. Lin and K. Takahashi, Competition between H_2O and $(H_2O)_2$ reactions with CH_2OO/CH_3CHOO, *Phys. Chem. Chem. Phys.*, 2016, **18**(6), 4557–4568.

39 P. Aplincourt and M. F. Ruiz-López, Theoretical Investigation of Reaction Mechanisms for Carboxylic Acid Formation in the Atmosphere, *J. Am. Chem. Soc.*, 2000, **122**(37), 8990–8997.

40 R. Crehuet, J. M. Anglada and J. M. Bofill, Tropospheric Formation of Hydroxymethyl Hydroperoxide, Formic Acid, H_2O_2, and OH from Carbonyl Oxide in the Presence of Water Vapor: A Theoretical Study of the Reaction Mechanism, *Chem.–Eur. J.*, 2001, **7**(10), 2227–2235.

41 B. Long, J. L. Bao and D. G. Truhlar, Atmospheric Chemistry of Criegee Intermediates: Unimolecular Reactions and Reactions with Water, *J. Am. Chem. Soc.*, 2016, **138**(43), 14409–14422.

42 L. Chen, W. Wang, L. Zhou, W. Wang, F. Liu, C. Li and J. Lü, Role of water clusters in the reaction of the simplest Criegee intermediate CH_2OO with water vapour, *Theor. Chem. Acc.*, 2016, **135**(11), 252.

43 B. Long, Y. Wang, Y. Xia, X. He, J. L. Bao and D. G. Truhlar, Atmospheric Kinetics: Bimolecular Reactions of Carbonyl Oxide by a Triple-Level Strategy, *J. Am. Chem. Soc.*, 2021, **143**(22), 8402–8413.

44 T. Zhang, X. Lan, R. Wang, S. Roy, Z. Qiao, Y. Lu and Z. Wang, The catalytic effects of H_2CO_3, CH_3COOH, HCOOH and H_2O on the addition reaction of CH_2OO + $H_2O \rightarrow CH_2(OH)OOH$, *Mol. Phys.*, 2018, **116**(14), 1783–1794.

45 T. B. Nguyen, J. D. Crounse, R. H. Schwantes, A. P. Teng, K. H. Bates, X. Zhang, J. M. St. Clair, W. H. Brune, G. S. Tyndall, F. N. Keutsch, J. H. Seinfeld and P. O. Wennberg, Overview of the Focused Isoprene eXperiment at the California Institute of Technology (FIXCIT): mechanistic chamber studies on the oxidation of biogenic compounds, *Atmos. Chem. Phys.*, 2014, **14**(24), 13531–13549.

46 T. Lewis, D. E. Heard and M. A. Blitz, A novel multiplex absorption spectrometer for time-resolved studies, *Rev. Sci. Instrum.*, 2018, **89**(2), 024101.

47 J. B. Burkholder, S. P. Sander, J. Abbatt, J. R. Barker, C. Cappa, J. D. Crounse, T. S. Dibble, R. E. Huie, C. E. Kolb, M. J. Kurylo, V. L. Orkin, C. J. Percival, D. M. Wilmouth, and P. H. Wine, *Chemical Kinetics and Photochemical Data for Use in Atmospheric Studies, Evaluation No. 19, JPL Publication 19-5*, Jet Propulsion Laboratory, Pasadena, 2019, **http://jpldataeval.jpl.nasa.gov**.

48 M. H. Harwood, J. B. Burkholder, M. Hunter, R. W. Fox and A. R. Ravishankara, Absorption Cross Sections and Self-Reaction Kinetics of the IO Radical, *J. Phys. Chem. A*, 1997, **101**(5), 853–863.

49 W.-L. Ting, Y.-H. Chen, W. Chao, M. C. Smith and J. J.-M. Lin, The UV absorption spectrum of the simplest Criegee intermediate CH_2OO, *Phys. Chem. Chem. Phys.*, 2014, **16**(22), 10438–10443.

50 M. C. Smith, C.-H. Chang, W. Chao, L.-C. Lin, K. Takahashi, K. A. Boering and J. J.-M. Lin, Strong Negative Temperature Dependence of the Simplest Criegee Intermediate CH_2OO Reaction with Water Dimer, *J. Phys. Chem. Lett.*, 2015, **6**(14), 2708–2713.

51 B. Ruscic, Active Thermochemical Tables: Water and Water Dimer, *J. Phys. Chem. A*, 2013, **117**(46), 11940–11953.

52 I. Bey, D. J. Jacob, R. M. Yantosca, J. A. Logan, B. D. Field, A. M. Fiore, Q. Li, H. Y. Liu, L. J. Mickley and M. G. Schultz, Global modeling of tropospheric chemistry with assimilated meteorology: Model description and evaluation, *J. Geophys. Res.: Atmos.*, 2001, **106**, 23073–23095.

53 R. Gelaro, W. McCarty, M. J. Suárez, R. Todling, A. Molod, L. Takacs, C. A. Randles, A. Darmenov, M. G. Bosilovich, R. Reichle, K. Wargan, L. Coy, R. Cullather, C. Draper, S. Akella, V. Buchard, A. Conaty, A. M. da Silva, W. Gu, G.-K. Kim, R. Koster, R. Lucchesi, D. Merkova, J. E. Nielsen, G. Partyka, S. Pawson, W. Putman, M. Rienecker, S. D. Schubert, M. Sienkiewicz and B. Zhao, The Modern-Era Retrospective Analysis for Research and Applications, Version 2 (MERRA-2), *J. Clim.*, 2017, **30**(14), 5419–5454.

54 K. H. Bates, D. J. Jacob, K. Li, P. D. Ivatt, M. J. Evans, Y. Yan and J. Lin, Development and evaluation of a new compact mechanism for aromatic oxidation in atmospheric models, *Atmos. Chem. Phys.*, 2021, **21**(24), 18351–18374.

55 A. B. Guenther, X. Jiang, C. L. Heald, T. Sakulyanontvittaya, T. Duhl, L. K. Emmons and X. Wang, The Model of Emissions of Gases and Aerosols from Nature version 2.1 (MEGAN2.1): an extended and updated framework for modeling biogenic emissions, *Geosci. Model Dev.*, 2012, **5**(6), 1471–1492.

56 G. R. van der Werf, J. T. Randerson, L. Giglio, T. T. van Leeuwen, Y. Chen, B. M. Rogers, M. Mu, M. J. E. van Marle, D. C. Morton, G. J. Collatz, R. J. Yokelson and P. S. Kasibhatla, Global fire emissions estimates during 1997–2016, *Earth Syst. Sci. Data*, 2017, **9**(2), 697–720.

57 R. M. Hoesly, S. J. Smith, L. Feng, Z. Klimont, G. Janssens-Maenhout, T. Pitkanen, J. J. Seibert, L. Vu, R. J. Andres, R. M. Bolt, T. C. Bond, L. Dawidowski, N. Kholod, J. I. Kurokawa, M. Li, L. Liu, Z. Lu, M. C. P. Moura, P. R. O'Rourke and Q. Zhang, Historical (1750–2014) anthropogenic emissions of reactive gases and aerosols from the Community Emissions Data System (CEDS), *Geosci. Model Dev.*, 2018, **11**(1), 369–408.

58 M. E. Jenkin, J. C. Young and A. R. Rickard, The MCM v3.3.1 degradation scheme for isoprene, *Atmos. Chem. Phys.*, 2015, **15**(20), 11433–11459.

59 K. H. Bates and D. J. Jacob, A new model mechanism for atmospheric oxidation of isoprene: global effects on oxidants, nitrogen oxides, organic products, and secondary organic aerosol, *Atmos. Chem. Phys.*, 2019, **19**(14), 9613–9640.

60 L. Onel, M. Blitz, P. Seakins, D. Heard and D. Stone, Kinetics of the Gas Phase Reactions of the Criegee Intermediate CH_2OO with O_3 and IO, *J. Phys. Chem. A*, 2020, **124**(31), 6287–6293.

61 P. O. Wennberg, K. H. Bates, J. D. Crounse, L. G. Dodson, R. C. McVay, L. A. Mertens, T. B. Nguyen, E. Praske, R. H. Schwantes, M. D. Smarte, J. M. St Clair, A. P. Teng, X. Zhang and J. H. Seinfeld, Gas-Phase Reactions of Isoprene and Its Major Oxidation Products, *Chem. Rev.*, 2018, **118**(7), 3337–3390.